

SAFARI: Versatile and Efficient Evaluations for Robustness of Interpretability

Wei Huang, Xingyu Zhao, Gaojie Jin, Xiaowei Huang

Department of Computer Science, University of Liverpool, Liverpool, L69 3BX, U.K.
 {w.huang23,xingyu.zhao,g.jin3,xiaowei.huang}@liverpool.ac.uk

Abstract

Interpretability of Deep Learning (DL) models is arguably the barrier in front of trustworthy AI. Despite great efforts made by the Explainable AI (XAI) community, explanations lack robustness—indistinguishable input perturbations may lead to different XAI results. Thus, it is vital to assess how robust DL interpretability is, given an XAI technique. To this end, we identify the following challenges that state-of-the-art is unable to cope with collectively: i) XAI techniques are highly heterogeneous; ii) misinterpretations are normally rare events; iii) both *worst-case* and *overall* robustness are of practical interest. In this paper, we propose two evaluation methods to tackle them—i) they are of black-box nature, based on Genetic Algorithm (GA) and Subset Simulation (SS); ii) bespoke fitness functions are used by GA to solve a constrained optimisation efficiently, while SS is dedicated to estimating rare event probabilities; iii) two diverse metrics are introduced, concerning the worst-case interpretation discrepancy and a probabilistic notion of *how* robust in general, respectively. We conduct experiments to study the accuracy, sensitivity and efficiency of our methods that outperform state-of-the-arts. Finally, we show two applications of our methods for ranking robust XAI methods and selecting training schemes to improve both classification and interpretation robustness.

1 Introduction

A key impediment to wide adoption of Deep Learning (DL) is their perceived lack of transparency, which promotes the rapid development of Explainable AI (XAI)—a research field that aims at improving the transparency and trust of AI. Typically, XAI techniques visualise which input features are significant to DL model’s prediction via, e.g., attribution maps (Arrieta et al. 2020; Huang et al. 2020; Zhang et al. 2021). However, interpretations¹ suffer from the lack of robustness. Many works have shown that a small perturbation can manipulate the interpretation while keeping model’s prediction unchanged, e.g., (Ghorbani, Abid, and Zou 2019; Kindermans et al. 2019). Moreover, there also exists the misinterpretation of Adversarial Examples (AEs) (Zhang et al. 2020), i.e., adversarial perturbations can not

¹Despite the subtle difference between interpretability and explainability, we use both terms interchangeably as an attribute of DL models in this paper. While, as suggested by (Molnar 2020), we use explanation/interpretation for individual predictions.

only fool DL’s prediction, but also the interpretation with respect to the misclassified² label so that the interpretation of the AE “remains” as that of the original input. To illustrate the aforementioned two types of misinterpretations, we refer readers to Fig. 1 for examples. In this regard, it is vital to assess how robust the coupled DL model and XAI method against input perturbations, which motivates this work.

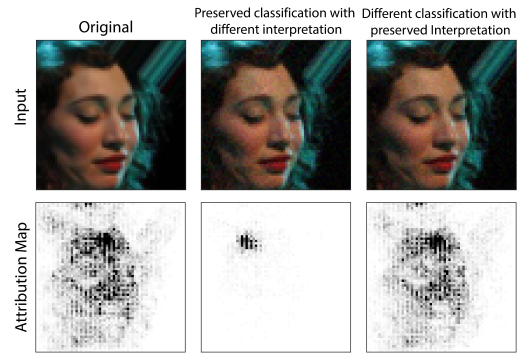


Figure 1: Two types of misinterpretations after perturbation

To answer the question, the 1st challenge we found is the need of diverse evaluation metrics that are missing from state-of-the-art. Most of existing works focus on adversarial attack on explanations (Heo, Joo, and Moon 2019; Slack et al. 2020) and defence (Dombrowski et al. 2022; Tang et al. 2022), which essentially answer the *binary* question of whether there exist any adversarial interpretation in some perturbation distance. On the other hand, evaluation approaches mainly study *extreme-case* metrics, e.g., the *maximum* change in the resulting explanations when perturbations are made (Alvarez-Melis and Jaakkola 2018) and local *Lipschitz continuity* as the sensitivity to perturbations (Yeh et al. 2019). However, for *systematic* evaluation, in addition to binary/worst-case metrics, we also need a notion of *how robust in general* the model is whenever a misinterpretation can be found (in line with the insight gained from evaluating classification robustness (Webb et al. 2019)). We introduce two metrics concerning the worst-case interpretation discrepancy and a probabilistic metric of the *proportion* of

²Without loss of generality, in this paper we assume the DL model is a classifier if with no further clarification.

misinterpretations in the local region around the original input, that complement each other from different perspectives.

Second, today’s XAI techniques are so heterogeneous (cf. Sec. 2.1 for a list) that no existing evaluation methods are generic enough to be applicable on all common ones. That said, white-box methods requiring internal information of DL models and/or XAI tools are hopeless, e.g. (Ghorbani, Abid, and Zou 2019; Zhang et al. 2020), while black-box evaluation is the only way forward. Based on this insight, we design a Genetic Algorithm (GA) and a statistical Subset Simulation (SS) approach to estimate the two robustness metrics introduced early, that both are of black-box nature.

The 3rd challenge we identified is that misinterpretations are normally rare events in a local norm-ball. Without white-box information like gradients, black-box methods have to leverage auxiliary information to detect such rare events efficiently. In our evaluations, we design bespoke fitness functions in the GA to solve an optimisation efficiently, and retrofit the established SS, dedicated to estimating rare event probabilities (Au and Beck 2001), for misinterpretation.

To the best of our knowledge, no state-of-the-arts can collectively cope with the three pinpointed challenges like ours. To validate the claim, we conduct experiments to study the accuracy, sensitivity and efficiency of our methods. Moreover, we develop two practical applications of our methods: i) We evaluate a wide range of XAI techniques and draw insights on their robustness; ii) Both theoretical analysis and empirical studies confirm the strong correlation between interpretation robustness and the curvature of DL model’s loss function (Dombrowski et al. 2019). It is also known that curvature regularisation may improve classification robustness (Moosavi-Dezfooli et al. 2019). Consequently, in this 2nd application, we ask, what is the intersection and gap between classification robustness and interpretation robustness? Is there any training scheme to improve both?

In summary, the key contributions of this paper include:

- Two diverse and novel metrics, worst-case misinterpretation discrepancy and probabilistic interpretation robustness, that complement each other as a holistic approach.
- GA and SS are introduced to estimate the new metrics, which are black-box and thus generic to most³ XAI tools. Despite of the rare-event nature of misinterpretations, GA and SS are designed to be efficient to detect them.
- A theoretical bound is derived to show how the Hessian of input loss, classification robustness and interpretation robustness are related, hinting good training schemes.
- Two practical applications of our methods for ranking robust XAI techniques, and selecting training schemes to improve both classification and interpretation robustness.

³Current version of our tool is applicable to the most common type of feature-attribution XAI methods, with a great potential to be modified for other types, e.g., rule/example based XAI. Moreover, we omit LIME (Ribeiro, Singh, and Guestrin 2016) and SHAP (Lundberg and Lee 2017) for brevity, because they require to utterly permute features of *each* perturbed input in a norm ball, generating a large number of samples in total, cf. Appendix for a detailed complexity analysis.

2 Preliminaries

2.1 Feature-Attribution based XAI

While readers are referred to (Arrieta et al. 2020; Huang et al. 2020) for a comprehensive review, we list some techniques fall into the common category of feature-attribution based XAI (Zhang et al. 2021) that studied by this work³.

Guided Backpropagation: It computes the gradient of output with respect to the input, but only the non-negative components of gradients are propagated to highlight the important pixels in the image (Springenberg et al. 2015).

Gradient \times Input: The map $g(x) = x \odot \frac{\partial f(x)}{\partial x}$ is more preferable to gradient alone to leverage the sign and strength of input to improve the interpretation sharpness (Shrikumar, Greenside, and Kundaje 2017).

Integrated Gradients: Instead of calculating single derivative, this approach integrates the gradients from some baseline to its current input value $g(x) = (x - \bar{x}) \int_{\alpha=0}^1 \frac{\partial f(\bar{x} + \alpha(x - \bar{x}))}{\partial x} d\alpha$, addressing the saturation and thresholding problems (Sundararajan, Taly, and Yan 2017).

Layer-wise Relevance Propagation (LRP): LRP operates by propagating the outputs $f(x)$ backwards, subject to the conservation rule (Bach et al. 2015). Given neurons j and k in two consecutive layers, propagating relevance score R_k to neurons j in lower layer can be expressed as $R_j = \sum_k \frac{z_{jk}}{\sum_j z_{jk}} R_k$ where weight $z_{jk} = w_{jk}x_k$ is the weighted activation, representing the contribution of relevance neuron k makes to neuron j .

DeepLift: It is an improved version of LRP by considering changes in the neuron activation from the reference point when propagating the relevance scores (Shrikumar, Greenside, and Kundaje 2017). Rescale rule is used to assign contribution scores to each neuron.

2.2 Local Robustness of Interpretation

Analogous to the robustness problem of classification, interpretation can be fooled by adding perturbations to the input. The interpretation robustness is highly related to the robustness of classification, since the attribution map is produced based on some prediction class. We first formalise the robustness of classification, and then define the robustness of interpretation. We have the following notations. Given an input seed x , we may find a norm ball $B(x, r)$ with the central point at x and radius r in L_p norm. We denote the prediction output of the DL model as the vector $f(x)$ with size equal to the total number of labels.

Robustness of classification requires that DL model’s prediction output should be invariant to the human imperceptible noise, which can be expressed through the prediction loss around an input seed x

$$J(f(x), f(x')) = \max_{i \neq y} (f_i(x') - f_y(x')) \quad (1)$$

$$y = \arg \max_i f_i(x), \quad x' \in B(x, r)$$

where $f_i(x')$ returns the probability of label i after input x' being processed by the DL model f . Note, $J \geq 0$ implies

that x' is an AE. We then define the following indicator function for misclassification within the norm ball $B(x, r)$

$$I_c = \begin{cases} -1 & \text{if } J(f(x), f(x')) \geq 0 \\ 1 & \text{if } J(f(x), f(x')) < 0 \end{cases} \quad (2)$$

That is, $I_c = -1$ indicates misclassification, otherwise 1.

Next, we define the robustness of interpretation. Previous works study two circumstances when small perturbation fools the interpretation $g(x)$, cf. Fig. 1 for examples. We use the interpretation discrepancy $\mathfrak{D}(g(x), g(x'))$ (defined later) to quantify the difference between the new interpretation $g(x')$ after perturbation and the reference $g(x)$, where $x' \in B(x, r)$. We then introduce two constants as thresholds, α and β , such that $\mathfrak{D} < \alpha$ represents consistent interpretations, while $\mathfrak{D} > \beta$ represents inconsistent interpretations⁴. The two misinterpretation regions within the norm ball $B(x, r)$ are then defined as

$$\hat{F} = \{\mathfrak{D} > \beta \wedge J < 0\}, \quad \tilde{F} = \{\mathfrak{D} < \alpha \wedge J \geq 0\} \quad (3)$$

\hat{F} represents preserved classification with different interpretation and \tilde{F} represents different classification with preserved interpretation, respectively. Note, α and β are hyperparameters that define the consistency notion of interpretations. They may vary case by case in the application specific context, representing the level of strictness required by the users on interpretation robustness.

2.3 Interpretation Discrepancy Metrics

In order to quantify the visual discrepancy between the XAI results (i.e., attribution maps), there are several commonly used metrics, including Mean Square Error (MSE), Pearson Correlation Coefficient (PCC), and Structural Similarity Index Measure (SSIM) (Dombrowski et al. 2019). PCC and SSIM have the absolute values in $[0, 1]$. The smaller values indicate the larger discrepancy between two interpretations. MSE calculates the average squared differences, the value of which more close to 0 means higher similarity. Then, interpretation discrepancy \mathfrak{D} can be expressed as

$$\mathfrak{D} = \frac{1}{\text{PCC}} \text{ or } \frac{1}{\text{SSIM}} \text{ or } \text{MSE} \quad (4)$$

3 Two Types of Robustness

Suppose the gradient based interpretation can be written as $g(x) = \nabla \ell(x)$, where ℓ can be the cross-entropy loss (or our defined prediction loss J). We leverage Lipschitz continuous gradient to hint the relation between classification robustness and interpretation robustness as what follows.

A differentiable function $\ell(x)$ is called smooth within local region $B(x, r)$ iff it has a Lipschitz continuous gradient, i.e., if $\exists K > 0$ such that

$$\|\nabla \ell(x') - \nabla \ell(x)\| \leq K \|x' - x\|, \quad \forall x' \in B(x, r). \quad (5)$$

Proposition 1 *Lipschitz continuous gradient implies:*

$$\|\ell(x') - \ell(x)\| \leq \|\nabla \ell(x)\| r + \frac{K}{2} r^2 \quad (6)$$

⁴When $\alpha \leq \mathfrak{D} \leq \beta$, it represents the case that we cannot clearly decide if the two interpretations are consistent or not.

Cf. Appendix for the proof. Proposition 1 says, the change of classification is bounded by input gradient $\|\nabla \ell(x)\|$, as well as $\frac{K}{2}$. K can be chosen as the Frobenius norm of input hessian $\|H\|_F(x)$ (Dombrowski et al. 2022). In later experiments, based on our metrics, we empirically study how the two regularisations of input gradient and input hessian affect classification robustness and interpretation robustness.

4 Related Work

Evaluation of Interpretation Robustness Existing evaluation metrics proposed for interpretation robustness only consider the misinterpretation when prediction label of perturbed inputs are unchanged. The work (Alvarez-Melis and Jaakkola 2018) estimates the Local Lipschitz of interpretation $g(x)$, while (Yeh et al. 2019) introduces the max-sensitivity and average-sensitivity of interpretation $g(x)$. Both of them use Simple Monte Carlo (SMC) sampling to estimate their metrics. In (Dasgupta, Frost, and Moshkovitz 2022), it defines the consistency as the probability that the inputs with the same interpretation have the same prediction label. However, their evaluation method is only applicable to tree ensemble models and tabular datasets with low dimensionality, leaving the probabilistic estimation of misinterpretation for high dimensional image dataset blank.

Notably, toolsets/benchmarks for evaluating XAI techniques are emerging in the last two years, including (Kokhlikyan et al. 2020; Agarwal et al. 2022; Liu et al. 2021; Arras, Osman, and Samek 2022). They are not specifically built for evaluating interpretation robustness, thus only concern the aforementioned metrics from (Alvarez-Melis and Jaakkola 2018) and (Yeh et al. 2019) and use SMC for estimation. While, our metrics complement theirs, and our GA and SS are more efficient than SMC.

Adversarial Attack and Defence on Interpretation

Ghorbani *et al.* first introduce the notion of adversarial perturbation to Neural Network (NN) interpretation (Ghorbani, Abid, and Zou 2019). Afterwards, several works are dedicated to generating indistinguishable inputs which have the same prediction label but substantially different interpretations (Heo, Joo, and Moon 2019; Slack et al. 2020). The theoretical analysis has shown that the lack of interpretation robustness is related to geometrical properties of NNs (Dombrowski et al. 2019). In (Zhang et al. 2020), a new class of attack is proposed to fool the NN’s prediction as well as the coupled XAI method.

In (Dombrowski et al. 2019), an upper bound on maximum changes of gradient-based interpretation is derived. The upper bound is proportional to the smooth parameter of the softplus activation function, which can be smoothed to improve the interpretation robustness. In (Dombrowski et al. 2022), regularisation on training, like weight decay, and minimising hessian of NNs are theoretically proved to be effective for training more robust NNs against interpretation manipulation. In (Zhao et al. 2021b), prior knowledge, e.g., from V&V evidence, is leveraged in Bayesian surrogate models for more robust and consistent XAI results.

5 Worst Case Evaluation

The conventional way to evaluate robustness of classification is based on the *worst case* loss under the perturbation (Yu et al. 2019). This underlines the adversarial attack and motivates the adversarial training. Similarly, *the worst case interpretation discrepancy between the original input and perturbed input may partly reflect interpretation robustness*.

There are two types of misinterpretations after perturbation in a local region, cf. Eq. (3). Two optimisation problems are formalised for the worst case interpretation discrepancy:

$$\text{sol}_{\hat{F}} = \max_{x' \in B(x,r)} \mathcal{D}(g(x), g(x')) \quad (7)$$

$$\text{s.t. } J(f(x), f(x')) < 0$$

$$\text{sol}_{\tilde{F}} = \min_{x' \in B(x,r)} \mathcal{D}(g(x), g(x')) \quad (8)$$

$$\text{s.t. } J(f(x), f(x')) \geq 0$$

That is, $\text{sol}_{\hat{F}}$ corresponds to finding the largest interpretation discrepancy when perturbed input is still correctly classified. While $\text{sol}_{\tilde{F}}$ is the minimum interpretation discrepancy between the AE x' and input seed x .

Previous works adopt white-box methods to solve the above optimisations for adversarial explanations (Zhang et al. 2020; Ghorbani, Abid, and Zou 2019), in which case the DL model $f(x)$ and XAI method $g(x)$ are required to be fully accessible to derive the gradient of interpretation discrepancy \mathcal{D} and prediction loss ℓ . In addition, XAI methods $g(x)$ are so heterogeneous that many of them are not differentiable, making white-box evaluations inapplicable. That said, we propose an black-box method, based on GA, to solve the constrained optimisation.

The core of GA is the design of fitness functions. At each iteration, the most fitted individuals are selected as parents for latter operations. GA can be directly applied to the unconstrained optimisation when objective function equals to fitness function. The constraint optimisation is more challenging and different strategies are proposed to handle the non-linear constraint for GA (Michalewicz and Schoenauer 1996). We refer readers to Appendix for more details of GA.

For the optimisation of (7), the constraint can be directly encoded as the indicator I_c into the fitness function

$$\mathcal{F} = I_c \mathcal{D}(g(x), g(x')) \quad (9)$$

and $\mathcal{D}(g(x), g(x'))$ is always none negative. All feasible individuals satisfying the constraint $J(f(x), f(x')) < 0$ will have $I_c = 1$, and $\mathcal{F} > 0$. If the constraint is violated, then $I_c = -1$, and $\mathcal{F} < 0$. In other words, the individuals violating the constraint will have smaller fitness values than the others and are suppressed during the evolution.

For the optimisation of (8), we note $J > 0$ is a rare event within the local region $B(x, r)$, as AEs are normally rare (Webb et al. 2019). To accelerate the search in the feasible input space, we set two fitness functions \mathcal{F}_1 and \mathcal{F}_2 . The former increases the proportion of AEs in the population. On this basis, when over half of the population are AEs, then \mathcal{F}_2 will guide the generation of adversarial explanations.

$$\mathcal{F}_1 = J(f(x), f(x')) \quad \mathcal{F}_2 = -I_c \mathcal{D}(g(x), g(x')) \quad (10)$$

In \mathcal{F}_2 , I_c also penalises the violation of constraints, which keeps the optimisation conditioned on AEs.

6 Probabilistic Evaluation

6.1 Probabilistic Metrics

In addition to the worst case metric, probabilistic evaluation based on statistical approaches is of the same (if not more) practical interest, which is a lesson learnt from evaluating classification robustness (Webb et al. 2019; Wang, Webb, and Rainforth 2021) and DL reliability (Zhao et al. 2021a). To this end, we study the *probability of misinterpretation* within $B(x, r)$ on the two types of misinterpretations⁵:

$$P(F) = \int_{x' \in B(x,r)} \mathbb{1}_F q(x') dx', \quad F = \hat{F} \text{ or } \tilde{F} \quad (11)$$

where x' is a randomly perturbed sample under the distribution $q(x')$ (precisely the ‘‘input model’’ used by, e.g. (Webb et al. 2019), when study local probabilistic metrics) in $B(x, r)$, and $\mathbb{1}_F$ is equal to 1 when F is true, 0 otherwise.

6.2 Estimation by Subset Simulation

To estimate the two probabilistic metrics defined by Eq. (11), we face two challenges: i) misinterpretations represented by \tilde{F} and \hat{F} are arguably rare events (that confirmed empirically later in our experiments); ii) inputs of DL models are usually high dimensional data-points like images. Thus, we need advanced sampling methods specifically designed for rare events, rather than SMC sampling (that is known to be inefficient for rare events). But still, some commonly used advanced sampling methods for rare events, like importance sampling, may not be applicable to high dimensional data (Au and Beck 2003).

The well-established Subset Simulation (SS) can efficiently calculate the small failure probability in high dimensional space (Au and Beck 2001). As a black-box method, it only involves the input and response of interest for calculation, thus generic to diverse XAI methods $g(x)$. The main idea of SS is introducing intermediate failure events so that the failure probability can be expressed as the product of larger conditional probabilities. Let $F = F_m \subset F_{m-1} \subset \dots \subset F_2 \subset F_1$ be a sequence of increasing events so that $F_k = \bigcap_{i=1}^k F_i$. By conditional probability, we get

$$P_F := P(F_m) = P\left(\bigcap_{i=1}^m F_i\right) = P(F_1) \prod_{i=1}^{m-1} P(F_{i+1}|F_i) \quad (12)$$

The conditional probabilities of intermediate events involved in Eq. (12) can be chosen sufficiently large so that they can be efficiently estimated. For example, $P(F_1) = P(F_{i+1}|F_i) = 0.1$, $i = 1, 2, 3, 4$, then $P_F \approx 10^{-5}$ which is too small for efficient estimation by SMC sampling. In this section, we adapt SS for our problem, as what follows.

Design of Intermediate Events \hat{F} and \tilde{F} can be decomposed as the series of intermediate events through the expression of property functions J and \mathcal{D} . For \hat{F} , $J < 0$ is

⁵Through out the paper, we use the shorthand notation F for either \hat{F} or \tilde{F} , according to the context.

not rare for a well-trained DL model, representing the correctly classified input after perturbation. Thus, the intermediate events \hat{F}_i and \hat{F}_{i+1} can be chosen as

$$\hat{F}_i = \{I_c \mathcal{D} > \beta_i\}, \quad \hat{F}_{i+1} = \{I_c \mathcal{D} > \beta_{i+1}\} \quad (13)$$

where $0 < \beta_i < \beta_{i+1} \leq \beta$

such that $\hat{F}_{i+1} \subset \hat{F}_i$. I_c (in Eq. 2) encodes the constraint $J < 0$ as the sign of \mathcal{D} .

In contrast, $J \geq 0$ in \tilde{F} represents the occurrence of AEs that are rare events, which cannot be directly expressed as the indicator I_c , since the random sampling within $B(x, r)$ cannot easily satisfy $J \geq 0$. Thus, for \tilde{F} , $J \geq 0$ should be chosen as the critical intermediate event.

$$\tilde{F}_j = \{J \geq 0\}, \quad \text{where } 1 < j < m \quad (14)$$

For intermediate events \tilde{F}_i and \tilde{F}_{i+1} , when $i+1 \leq j$, we set

$$\tilde{F}_i = \{J > \gamma_i\}, \quad \tilde{F}_{i+1} = \{J > \gamma_{i+1}\} \quad (15)$$

where $\gamma_i < \gamma_{i+1} < 0$

such that $\tilde{F}_j \subset \tilde{F}_{i+1} \subset \tilde{F}_i$. And for intermediate events \tilde{F}_k and \tilde{F}_{k+1} , when $k > j$, we can set

$$\tilde{F}_k = \{-I_c/\mathcal{D} > 1/\alpha_k\}, \quad \tilde{F}_{k+1} = \{-I_c/\mathcal{D} > 1/\alpha_{k+1}\} \quad (16)$$

where $0 < \alpha \leq \alpha_{k+1} < \alpha_k$

such that $\tilde{F}_{k+1} \subset \tilde{F}_k \subset \tilde{F}_j$.

Estimating Conditional Probabilities Upon formally defined intermediate events, the question arises on how to set β_i , γ_i and α_i to make the conditional probability $P(F_{i+1}|F_i)$ sufficiently large for estimation by a few simulations. Also, $P(F_{i+1}|F_i)$ cannot be efficiently estimated by common technique due to the rarity of F_{i+1} . Therefore, the Markov Chain Monte Carlo sampling based on the Metropolis–Hastings (MH) algorithm is adopted. For simplicity, the intermediate event threshold is generally denoted as $L_i = \{\beta_i, \gamma_i, \alpha_i\}$.

Choices of Intermediate Event Threshold Start from estimating $P(F_1)$, F_1 is chosen as the common event such that N samples are drawn from $q(\cdot)$ by SMC and all belong to F_1 . A feasible way is setting the threshold of property function L_1 to $-\infty$, and $P(F_1) = 1$. For $i = 2, \dots, m$, L_i affects the values of condition probabilities and hence the efficiency of SS. It is suggested that L_i is set adaptively to make $P(F_{i+1}|F_i)$ approximately equals to ρ , and ρ is a hyperparameter in SS (that takes a decimal less than 1 and normally can be empirically optimised), i.e., $P(F_{i+1}|F_i) \approx \rho$. In other words, at each iteration when we simulate N samples, ρN samples should belong to F_{i+1} .

Simulating New Samples from $q(\cdot|F_i)$ At iteration $i = 2, \dots, m$, we already have ρN samples belonging to F_i and aim to simulate new samples to enlarge the set to N , so that the conditional probability $P(F_{i+1}|F_i) = \frac{1}{N} \sum_{k=1}^N \mathbb{1}_{F_{i+1}}(x'_k)$ can be calculated. We can pick up an existing sample x' subject to the conditional distribution

$q(\cdot|F_i)$, denoted as $x' \sim q(\cdot|F_i)$, and use the MH algorithm to construct a Markov Chain. By running M steps of MH, the stationary distribution of the Markov Chain is $q(\cdot|F_i)$. Then new data $x'' \sim q(\cdot|F_i)$ can be sampled from the Markov Chain and added into the set. More details of the MH algorithm for SS are presented in Appendix.

Termination Condition and Returned Estimation By conducting the aforementioned steps, SS divides the problem of estimating a rare event probability into several simpler ones—a sequence of intermediate conditional probabilities, as formulated in Eq. (12). Since each conditional probability $P(F_{i+1}|F_i)$ approximately equals to ρ , then by Eq. (12), the returned estimation $\bar{P}_F \approx \rho^{m-1}$, where m is the total number of intermediate event generated adaptively. The adaptive generation of intermediate events terminates when $\bar{P}_F < P_{\min}$, and P_{\min} is a given termination threshold.

7 Experiments

7.1 Experiment Setup

We consider three public benchmark datasets⁶, five XAI methods, and five training schemes in our experiments. The norm ball radius, deciding the oracle of robustness, is calculated with respect to the r separation property (Yang et al. 2020). That is, $r = 0.3$ for MNIST, $r = 0.03$ for CIFAR10, and $r = 0.05$ for CelebA. More details of the DL models under study are presented in Appendix. For the probabilistic evaluation using SS, without loss of generality, we consider the uniform distribution as $q(x')$ within each norm ball. We compare $\mathcal{D} = \text{MSE}$, $1/\text{PCC}$, and $1/\text{SSIM}$ for measuring interpretation discrepancy in Appendix, and find PCC is better to quantify the interpretation difference in our cases. Based on sensitivity analysis, we choose hyperparameters PCC thresholds $1/\beta = 0.4$, $1/\alpha = 0.6$, MH steps $M = 250$, $\ln P_{\min} = -100$ for probabilistic evaluation, and population size $N = 1000$, number of iteration $itr = 500$ for the worst case evaluation by GA. Our tools are publicly available at https://github.com/havelhuang/Eval_XAI_Robustness.

7.2 Sensitivity to Hyper-Parameter Settings

We first investigate the sensitivity of objective function \mathcal{D} and constraint J (cf. Eq. (7) and (8)) to GA’s population size and iteration numbers, as shown in Fig. 2. We observe from the 1st row that interpretation discrepancy measured by PCC (the red curve) quickly converge after 300 iterations with the satisfaction of constraint J (the blue curve), showing the effectiveness of our GA. From the 2nd row, we notice that the optimisation is not sensitive to population size, compared with the number of iterations, i.e., population size over 500 cannot make significant improvement to the optimisation. In addition, if the number of iterations is enough for achieving convergence results, the effect of population size on optimal solution further decreases. We only present the results of one seed from CelebA, cf. Appendix for more seeds from other datasets and the general observation/conclusion remains.

⁶Our methods work for all common data types like tabular data, text and images, while we focus on more challenging high-dimensional image data in our experiments.

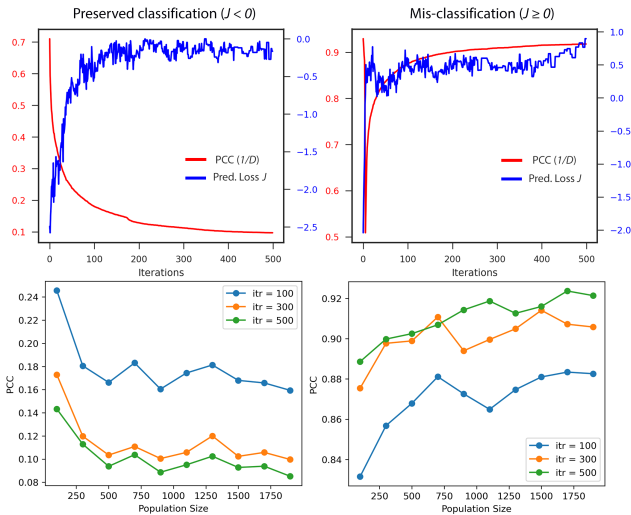


Figure 2: Sensitivity of objective function \mathcal{D} and constraint J to GA’s population size and iteration numbers. Each column represents a type of misinterpretation. 1st row: quickly converged GA objective functions satisfying the constraint, with fixed population size of 1000 and varying iterations. 2nd row: GA solutions, with fixed iteration numbers and varying population size. A test seed (a norm ball) from CelebA is used; interpretation discrepancy \mathcal{D} is measured by $1/\text{PCC}$; “Gradient \times Input” XAI method is studied.

Next, we study the sensitivity of SS accuracy to the number of MH steps M , varying the PCC threshold that defines the rarity level of misinterpretation events. In Fig. 3, we can calculate the difference $\Delta \ln P_F$ between SS estimations and SMC estimations (using a sufficiently large number of samples⁷). While the 1st row shows the overlapping of SS and SMC estimations (two red curves) and the decreasing running time (the blue curve) when decreasing the rarity levels of misinterpretations (i.e. PCC thresholds), we also observe from the 2nd row that, with increased MH steps M , the estimation accuracy of SS is significantly improved. In addition, the rarity of misinterpretation events determines the choice of M . E.g., if $\ln P_{\hat{F}} = -3.87$ with $\hat{F} = \{PCC < 0.4 \wedge J < 0\}$, then $M = 100$ already achieves high precision without additional sampling budget. Other parameters, e.g. the number of samples n and sample quantile ρ that are discussed in Appendix, are in general less sensitive than the number of MH steps M .

In summary, such sensitivity analysis provides the basis of setting hyper-parameters in later experiments: 500 iterations and 1000 population size for GA, 250 MH steps for SS.

7.3 Evaluation Accuracy and Efficiency

We study the accuracy of our GA-based evaluation, comparing with state-of-the-art (Alvarez-Melis and Jaakkola 2018; Yeh et al. 2019)—they define the local Lipschitz ($SENS_{LIPS}$)

⁷Specifically, we use 10^8 samples which can accurately estimate a small probability in natural logarithm around $-17 \sim -18$.

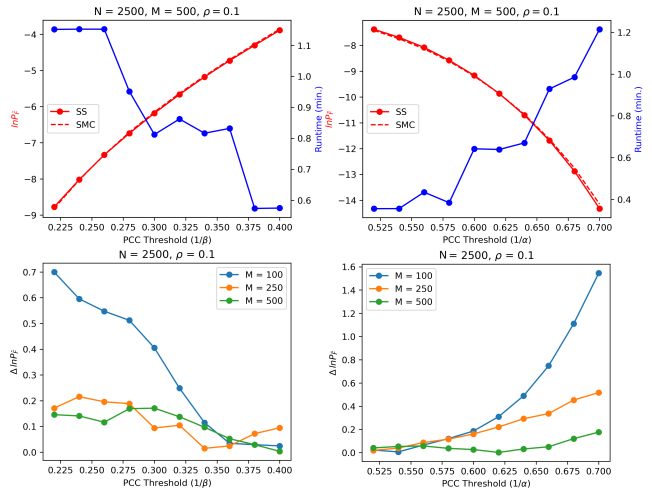


Figure 3: Each column represents a type of misinterpretation. 1st row: the probability of misinterpretation ($\ln P_F$) estimations returned by SS and SMC⁷ (~ 22 minutes for each estimate), varying the rarity of misinterpretations. Two estimations overlap showing high accuracy of SS. 2nd row: sensitivity of SS accuracy $\Delta \ln P_F$ to MH steps M , varying the rarity level of misinterpretation controlled by PCC threshold. A test seed from MNIST is used; Results are averaged over 10 runs; “Gradient \times Input” XAI method is considered.

and max-sensitivity ($SENS_{MAX}$) metrics for the maximum interpretation discrepancy, and empirically estimate the metrics using SMC sampling. For fair comparisons, we first choose MSE as the interpretation discrepancy metric in our fitness functions of GA, and then apply both GA and SMC to generate two populations of interpretations in which we calculate the 3 robustness metrics respectively and summarise in Table 1. We use 5×10^5 samples for both GA and SMC.

Table 1: Three worst case robustness metrics estimated by our GA and SMC, averaged over 100 test seeds. GA outperforms SMC (used by state-of-the-arts) w.r.t. all 3 metrics.

Dataset	GA			SMC		
	$sol_{\hat{F}}$ (MSE)	$SENS_{MAX}$	$SENS_{LIPS}$	$sol_{\hat{F}}$ (MSE)	$SENS_{MAX}$	$SENS_{LIPS}$
MNIST	1.549	36.067	13.747	0.271	15.226	2.772
CIFAR10	42.436	328.147	314.861	0.589	38.529	40.232
CelebA	3.204	192.203	65.635	0.013	11.298	3.563

As shown in Table 1, our GA-based estimator outperforms SMC in all the three robustness metrics. Although the metrics of local Lipschitz and max-sensitivity are not explicitly encoded as optimisation objectives in our GA, still GA is more effective and efficient to estimate those three extreme values than SMC. This is non-surprising, since all three metrics are compatible and essentially representing the same worst-case semantics. That said, our new metric encoded by the GA could be more versatile than $SENS_{LIPS}$ and $SENS_{MAX}$ (in L_2 norm) via encoding other types of discrepancy metrics like PCC and SSIM.

For SS, in addition to the accuracy shown in Fig. 3, the

rarity of events (controlled by the PCC threshold) affects the running time per estimation. SS is a dedicated method for rare events, thus expected to be much more efficient than SMC. Indeed, SS takes less than 2 minutes on average for an estimation, while SMC takes ~ 22 minutes on average.

7.4 Evaluating XAI Methods

Based on our methods, the first application is to draw insights on the robustness of common XAI methods, from both the worst-case and probabilistic perspectives. Thanks to the black-box nature of GA and SS, our methods are applicable to diverse XAI tools, and we consider five most popular ones in this paper. We randomly sample 100 test seeds from MNIST for evaluations, and summarise the statistics in the box-and-whisker plots of Fig. 4. More results from CIFAR10 and CelebA are presented in Appendix.

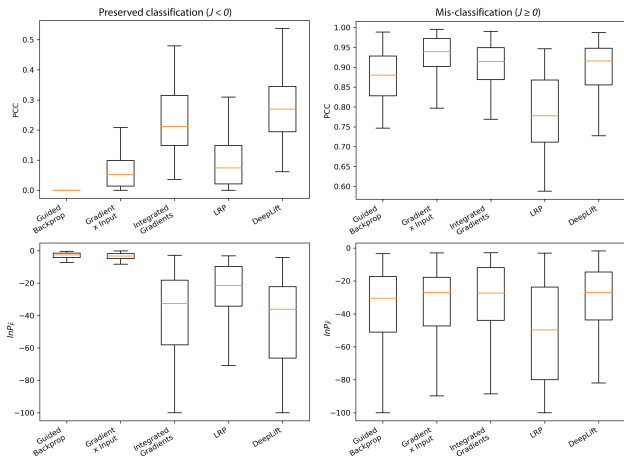


Figure 4: Worst-case (1st row) and probabilistic (2nd row) robustness evaluations of five XAI methods based on 100 random test seeds from MNIST. Each column represents a type of misinterpretation— \hat{F} left and \tilde{F} right. For top-left plot, higher value means more robust; for all other plots, lower value means more robust.

Based on the empirical results of Fig. 4, we may conclude: i) for misinterpretation \hat{F} —correct classification ($J < 0$) with inconsistent interpretation ($PCC < 0.4$), DeepLift and Integrated Gradients outperform others, while Guided Backprop and Gradient \times Input are unrobust both in worst-case and probabilistically; ii) for misinterpretation \tilde{F} —wrong classification ($J \geq 0$) with persevered interpretation ($PCC > 0.6$), while all XAI methods perform similarly w.r.t. both metrics, LRP shows better robustness than others.

The empirical insights are as expected if we consider the mechanisms behind those XAI methods. For instance, considering \hat{F} , DeepLift and Integrated Gradients are more robust, since they use the reference point to avoid the discontinuous gradients (large curvature) that mislead the attribution maps (Shrikumar, Greenside, and Kundaje 2017). On the other hand, DeepLift and Integrated Gradients become vulnerable to \tilde{F} . Because misclassification and misinterpretation are rare events, it is very likely that perturbed inputs

inside the norm ball have consistent interpretation with the seed. Consequently, the integration from the reference point which averages the attribution map over several points are prone to produce the consistent interpretations. We discuss more in Appendix to back up the empirical observations.

7.5 Evaluating Training Schemes

In this application, we study the effect of various training schemes on the classification robustness and interpretation robustness of DL models. As discussed in Sec. 3, input Hessian norm and input gradient norm are related to the change of classification loss and interpretation discrepancy. Thus, we add input gradient and hessian regularisation terms to the training loss, and also consider the PGD-based adversarial training (that improves classification robustness through minimising the maximal prediction loss in norm balls). Table 2 records the results.

Table 2: Evaluating classification (c) and interpretation (\hat{F} and \tilde{F}) robustness of DL models trained with input gradient norm regularisation (Grad. Reg.), input hessian norm regularisation (Hess. Reg.), both of them (Grad. + Hess. Reg.) and adversarial training (Adv. Train.). Results are averaged over 100 random test seeds. Higher $sol_{\hat{F}}$ means more robust, for other metrics, lower values means more robust.

Dataset	Model	Worst Case Evaluation			Probabilistic Evaluation		
		sol_c (J)	$sol_{\hat{F}}$ (PCC)	$sol_{\tilde{F}}$ (PCC)	$\ln P_c$	$\ln P_{\hat{F}}$	$\ln P_{\tilde{F}}$
MNIST	Org.	22.43	0.06	0.93	-24.28	-3.87	-31.47
	Grad. Reg.	11.37	0.10	0.92	-31.51	-15.69	-44.96
	Hess. Reg.	10.59	0.17	0.90	-33.36	-21.27	-43.85
	Grad. + Hess.	10.04	0.20	0.90	-36.96	-23.79	-46.19
	Adv. Train.	-0.16	0.21	0.59	-84.15	-28.67	-89.09
CIFAR10	Org.	42.58	0.02	0.85	-31.55	-18.63	-71.46
	Grad. Reg.	42.34	0.01	0.85	-27.31	-21.77	-65.75
	Hess. Reg.	8.99	0.08	0.81	-76.29	-99.20	-91.89
	Grad. + Hess.	8.47	0.06	0.81	-71.65	-98.49	-92.39
	Adv. Train.	-0.67	0.25	0.80	-92.57	-100	-95.97
CelebA	Org.	51.08	0.08	0.86	-13.77	-21.58	-70.82
	Grad. Reg.	25.29	0.06	0.88	-45.52	-70.22	-83.26
	Hess. Reg.	18.71	0.09	0.86	-74.93	-100	-95.85
	Grad. + Hess.	25.41	0.06	0.88	-65.95	-100	-94.13
	Adv. Train.	-0.45	0.55	0.81	-95.09	-100	-95.58

In addition to the knowledge that input hessian can defence adversarial interpretation (Dombrowski et al. 2022), we notice it is actually effective in improving both classification and interpretation robustness, than input gradient regularisation, confirming Proposition 1. Moreover, we discover that adversarial training is surprisingly effective at improving interpretation robustness, but at the price of dropping accuracy, cf. Appendix. Thus, there is no silver bullet training scheme that is effective for all DL attributes.

8 Conclusion

In this paper, we propose two versatile and efficient evaluation methods for DL interpretation robustness. We conclude versatile in two folds: the proposed metrics are characterising robustness from both worst-case and probabilistic perspectives, and GA and SS are black-box thus generic to heterogeneous XAI methods. Considering the rare-event nature of misinterpretations, GA and SS are designed to be efficient in detecting them, and shown with experimental results.

References

- Agarwal, C.; Saxena, E.; Krishna, S.; Pawelczyk, M.; Johnson, N.; Puri, I.; Zitnik, M.; and Lakkaraju, H. 2022. OpenXAI: Towards a Transparent Evaluation of Model Explanations. *arXiv preprint arXiv:2206.11104*.
- Alvarez-Melis, D.; and Jaakkola, T. S. 2018. On the robustness of interpretability methods. *arXiv preprint arXiv:1806.08049*.
- Arras, L.; Osman, A.; and Samek, W. 2022. CLEVR-XAI: A benchmark dataset for the ground truth evaluation of neural network explanations. *Information Fusion*, 81: 14–40.
- Arrieta, A. B.; Díaz-Rodríguez, N.; Ser, J. D.; Bennetot, A.; Tabik, S.; Barbado, A.; Garcia, S.; Gil-Lopez, S.; Molina, D.; Benjamins, R.; Chatila, R.; and Herrera, F. 2020. Explainable Artificial Intelligence (XAI): Concepts, taxonomies, opportunities and challenges toward responsible AI. *Information Fusion*, 58: 82–115.
- Au, S.-K.; and Beck, J. 2003. Important sampling in high dimensions. *Structural safety*, 25(2): 139–163.
- Au, S.-K.; and Beck, J. L. 2001. Estimation of small failure probabilities in high dimensions by subset simulation. *Probabilistic engineering mechanics*, 16(4): 263–277.
- Bach, S.; Binder, A.; Montavon, G.; Klauschen, F.; Müller, K.-R.; and Samek, W. 2015. On pixel-wise explanations for non-linear classifier decisions by layer-wise relevance propagation. *PLoS one*, 10(7): e0130140.
- Cérou, F.; Del Moral, P.; Furon, T.; and Guyader, A. 2012. Sequential Monte Carlo for rare event estimation. *Statistics and computing*, 22(3): 795–808.
- Chen, J.; Su, M.; Shen, S.; Xiong, H.; and Zheng, H. 2019. POBA-GA: Perturbation optimized black-box adversarial attacks via genetic algorithm. *Comput. Secur.*, 85: 89–106.
- Dasgupta, S.; Frost, N.; and Moshkovitz, M. 2022. Framework for Evaluating Faithfulness of Local Explanations. *arXiv preprint arXiv:2202.00734*.
- Dombrowski, A.-K.; Alber, M.; Anders, C.; Ackermann, M.; Müller, K.-R.; and Kessel, P. 2019. Explanations can be manipulated and geometry is to blame. *Advances in Neural Information Processing Systems*, 32.
- Dombrowski, A.-K.; Anders, C. J.; Müller, K.-R.; and Kessel, P. 2022. Towards robust explanations for deep neural networks. *Pattern Recognition*, 121: 108194.
- Gelman, A.; Gilks, W. R.; and Roberts, G. O. 1997. Weak convergence and optimal scaling of random walk Metropolis algorithms. *The annals of applied probability*, 7(1): 110–120.
- Ghorbani, A.; Abid, A.; and Zou, J. 2019. Interpretation of Neural Networks Is Fragile. *Proc. of the AAAI Conference on Artificial Intelligence*, 33(01): 3681–3688.
- Heo, J.; Joo, S.; and Moon, T. 2019. Fooling neural network interpretations via adversarial model manipulation. *Advances in Neural Information Processing Systems*, 32.
- Huang, X.; Kroening, D.; Ruan, W.; Sharp, J.; Sun, Y.; Thamo, E.; Wu, M.; and Yi, X. 2020. A survey of safety and trustworthiness of deep neural networks: Verification, testing, adversarial attack and defence, and interpretability. *Computer Science Review*, 37: 100270.
- Katafygiotis, L. S.; and Zuev, K. M. 2008. Geometric insight into the challenges of solving high-dimensional reliability problems. *Probabilistic Engineering Mechanics*, 23(2-3): 208–218.
- Kindermans, P.-J.; Hooker, S.; Adebayo, J.; Alber, M.; Schütt, K. T.; Dähne, S.; Erhan, D.; and Kim, B. 2019. The (Un)reliability of Saliency Methods. In *Explainable AI: Interpreting, Explaining and Visualizing Deep Learning*, 267–280. Cham: Springer. ISBN 978-3-030-28954-6.
- Kokhlikyan, N.; Miglani, V.; Martin, M.; Wang, E.; Alsallakh, B.; Reynolds, J.; Melnikov, A.; Kliushkina, N.; Araya, C.; Yan, S.; and Reblitz-Richardson, O. 2020. Captum: A unified and generic model interpretability library for PyTorch. *arXiv:2009.07896*.
- Konak, A.; Coit, D. W.; and Smith, A. E. 2006. Multi-objective optimization using genetic algorithms: A tutorial. *Reliability engineering & system safety*, 91(9): 992–1007.
- Lipowski, A.; and Lipowska, D. 2012. Roulette-wheel selection via stochastic acceptance. *Physica A: Statistical Mechanics and its Applications*, 391(6): 2193–2196.
- Liu, Y.; Khandagale, S.; White, C.; and Neiswanger, W. 2021. Synthetic Benchmarks for Scientific Research in Explainable Machine Learning. In *35th Conference on Neural Information Processing, Systems Datasets and Benchmarks Track*.
- Lundberg, S. M.; and Lee, S.-I. 2017. A unified approach to interpreting model predictions. *Advances in neural information processing systems*, 30.
- Michalewicz, Z.; and Schoenauer, M. 1996. Evolutionary algorithms for constrained parameter optimization problems. *Evolutionary computation*, 4(1): 1–32.
- Molnar, C. 2020. *Interpretable Machine Learning: A Guide for Making Black Box Models Explainable*. E-book on leanpub.com.
- Moosavi-Dezfooli, S.-M.; Fawzi, A.; Uesato, J.; and Frossard, P. 2019. Robustness via curvature regularization, and vice versa. In *Proceedings of the IEEE/CVF Conference on Computer Vision and Pattern Recognition*, 9078–9086.
- Papaioannou, I.; Betz, W.; Zwirgmaier, K.; and Straub, D. 2015. MCMC algorithms for subset simulation. *Probabilistic Engineering Mechanics*, 41: 89–103.
- Powell, D.; and Skolnick, M. M. 1993. Using Genetic Algorithms in Engineering Design Optimization with Non-Linear Constraints. In *Proceedings of the 5th International Conference on Genetic Algorithms*, 424–431. San Francisco, CA, USA: Morgan Kaufmann Publishers Inc.
- Ribeiro, M. T.; Singh, S.; and Guestrin, C. 2016. “Why Should I Trust You?”: Explaining the Predictions of Any Classifier. In *Proc. of the 22nd ACM SIGKDD International Conference on Knowledge Discovery and Data Mining*, KDD ’16, 1135–1144. New York, NY, USA: ACM.
- Schueller, G. I.; Pradlwarter, H. J.; and Koutsourelakis, P.-S. 2004. A critical appraisal of reliability estimation procedures for high dimensions. *Probabilistic engineering mechanics*, 19(4): 463–474.

Shrikumar, A.; Greenside, P.; and Kundaje, A. 2017. Learning important features through propagating activation differences. In *International conference on machine learning*, 3145–3153. PMLR.

Slack, D.; Hilgard, S.; Jia, E.; Singh, S.; and Lakkaraju, H. 2020. Fooling lime and shap: Adversarial attacks on post hoc explanation methods. In *Proceedings of the AAAI/ACM Conference on AI, Ethics, and Society*, 180–186.

Springenberg, J.; Dosovitskiy, A.; Brox, T.; and Riedmiller, M. 2015. Striving for Simplicity: The All Convolutional Net. In *ICLR (workshop track)*.

Sundararajan, M.; Taly, A.; and Yan, Q. 2017. Axiomatic attribution for deep networks. In *International conference on machine learning*, 3319–3328. PMLR.

Tang, R.; Liu, N.; Yang, F.; Zou, N.; and Hu, X. 2022. Defense Against Explanation Manipulation. *Frontiers in Big Data*, 5.

Wang, B.; Webb, S.; and Rainforth, T. 2021. Statistically robust neural network classification. In *Proc. of the Thirty-Seventh Conference on Uncertainty in Artificial Intelligence*, volume 161 of UAI'21 of PMLR, 1735–1745.

Webb, S.; Rainforth, T.; Teh, Y. W.; and Kumar, M. P. 2019. A Statistical Approach to Assessing Neural Network Robustness. In *7th Int. Conf. on Learning Representations (ICLR'19)*. OpenReview.net.

Yang, Y.-Y.; Rashtchian, C.; Zhang, H.; Salakhutdinov, R. R.; and Chaudhuri, K. 2020. A closer look at accuracy vs. robustness. *Advances in neural information processing systems*, 33: 8588–8601.

Yeh, C.-K.; Hsieh, C.-Y.; Suggala, A.; Inouye, D. I.; and Ravikumar, P. K. 2019. On the (in) fidelity and sensitivity of explanations. *Advances in Neural Information Processing Systems*, 32.

Yu, F.; Qin, Z.; Liu, C.; Zhao, L.; Wang, Y.; and Chen, X. 2019. Interpreting and evaluating neural network robustness. In *Proceedings of the 28th International Joint Conference on Artificial Intelligence*, 4199–4205.

Zhang, X.; Wang, N.; Shen, H.; Ji, S.; Luo, X.; and Wang, T. 2020. Interpretable Deep Learning under Fire. In *29th USENIX Security Symposium*, USENIX Security 20. USENIX Association.

Zhang, Y.; Tiño, P.; Leonardis, A.; and Tang, K. 2021. A survey on neural network interpretability. *IEEE Transactions on Emerging Topics in Computational Intelligence*.

Zhao, X.; Huang, W.; Banks, A.; Cox, V.; Flynn, D.; Schewe, S.; and Huang, X. 2021a. Assessing the Reliability of Deep Learning Classifiers Through Robustness Evaluation and Operational Profiles. In *AISafety'21 Workshop at IJCAI'21*, volume 2916. ceur-ws.org.

Zhao, X.; Huang, W.; Huang, X.; Robu, V.; and Flynn, D. 2021b. BayLIME: Bayesian local interpretable model-agnostic explanations. In *Proc. of the 37th Conference on Uncertainty in Artificial Intelligence*, volume 161 of UAI'21, 887–896. PMLR.

9 Appendix

9.1 Proof of Proposition 1

We first show that for $K > 0$, $\|\nabla\ell(x_1) - \nabla\ell(x_2)\| \leq K\|x_1 - x_2\|$ implies

$$\ell(x_1) - \ell(x_2) \leq \nabla\ell(x_2)^T(x_1 - x_2) + \frac{K}{2}\|x_1 - x_2\|^2$$

Recall from the integral calculus $\ell(a) - \ell(b) = \int_b^a \nabla\ell(\theta) d\theta$,

$$\begin{aligned} \ell(x_1) - \ell(x_2) &= \\ &\int_0^1 \nabla\ell(x_2 + \tau(x_1 - x_2))^T(x_1 - x_2) d\tau = \\ &\int_0^1 (\nabla\ell(x_2 + \tau(x_1 - x_2))^T - \nabla\ell(x_2)^T + \nabla\ell(x_2)^T) \\ &(x_1 - x_2) d\tau \end{aligned}$$

As $\nabla\ell(x_2)$ is independent of τ , it can be taken out from the integral

$$\begin{aligned} \ell(x_1) - \ell(x_2) &= \nabla\ell(x_2)^T(x_1 - x_2) + \\ &\int_0^1 (\nabla\ell(x_2 + \tau(x_1 - x_2))^T - \nabla\ell(x_2)^T)(x_1 - x_2) d\tau \end{aligned}$$

Then we move $\nabla\ell(x_2)^T(x_1 - x_2)$ to the left and get the absolute value

$$\begin{aligned} |\ell(x_1) - \ell(x_2) - \nabla\ell(x_2)^T(x_1 - x_2)| &= \\ &|\int_0^1 (\nabla\ell(x_2 + \tau(x_1 - x_2))^T - \nabla\ell(x_2)^T)(x_1 - x_2) d\tau| \leq \\ &\int_0^1 |(\nabla\ell(x_2 + \tau(x_1 - x_2))^T - \nabla\ell(x_2)^T)(x_1 - x_2)| d\tau \leq \text{c.s.} \\ &\int_0^1 \|(\nabla\ell(x_2 + \tau(x_1 - x_2)) - \nabla\ell(x_2))\| \|x_1 - x_2\| d\tau \end{aligned}$$

c.s. means Cauchy – Schwarz inequality. By applying Lipschitz continuous gradient, we can get

$$\begin{aligned} \|(\nabla\ell(x_2 + \tau(x_1 - x_2)) - \nabla\ell(x_2))\| & \\ &\leq K\|\tau(x_1 - x_2)\| \\ &\leq K\tau\|x_1 - x_2\| \end{aligned}$$

Note $\tau \geq 0$, and the absolute sign of τ can be removed. Then, we can get

$$\begin{aligned} |\ell(x_1) - \ell(x_2) - \nabla\ell(x_2)^T(x_1 - x_2)| &\leq \\ &\int_0^1 K\tau\|x_1 - x_2\|^2 d\tau = \frac{K}{2}\|x_1 - x_2\|^2 \end{aligned}$$

Next, get the norm of two sides, and apply triangle inequality, we finally get

$$\begin{aligned} \|\ell(x') - \ell(x)\| &\leq \|\nabla\ell(x)^T(x' - x) + \frac{K}{2}\|x' - x\|^2\| \\ &\leq \|\nabla\ell(x)\| \|x' - x\| + \frac{K}{2}\|x' - x\|^2 \\ &\leq \|\nabla\ell(x)\| r + \frac{K}{2}r^2 \end{aligned} \tag{17}$$

QED

9.2 Genetic Algorithm based Optimisation

Genetic Algorithm (GA) is a classic evolutionary algorithm for solving the either constrained or unconstrained optimisation problems. It mimics the biological evolution by selecting the most fitted individuals in the population, which will be the parents for the next generation. It consists of 4 steps: initialisation, selection, crossover, and mutation, the last three of which are repeated until the convergence of fitness values.

Initialisation The initialisation of population is crucial to the quick convergence. Diversity of initial population could promise approximate global optimal (Konak, Coit, and Smith 2006). Normally, we use the Gaussian distribution with the mean at input seed x , or a uniform distribution to generate a set of diverse perturbed inputs within the norm ball $B(x, r)$.

Selection A fitness function is defined to select fitted individuals as parents for the latter operations. We use the fitness proportionate selection (Lipowski and Lipowska 2012).

$$p_i = \frac{\mathcal{F}_i}{\sum_{i=1}^n \mathcal{F}_i} \tag{18}$$

The fitness value is used to associate a probability of selection p_i for each individuals to maintaining good diversity of population and avoid premature convergence. The fitness function is the objective function to be optimised. For example, previous paper applies GA to the perturbation optimisation to generate the high quality AEs (Chen et al. 2019). In this paper, the explanation discrepancy is optimised to find the worst case adversarial explanations.

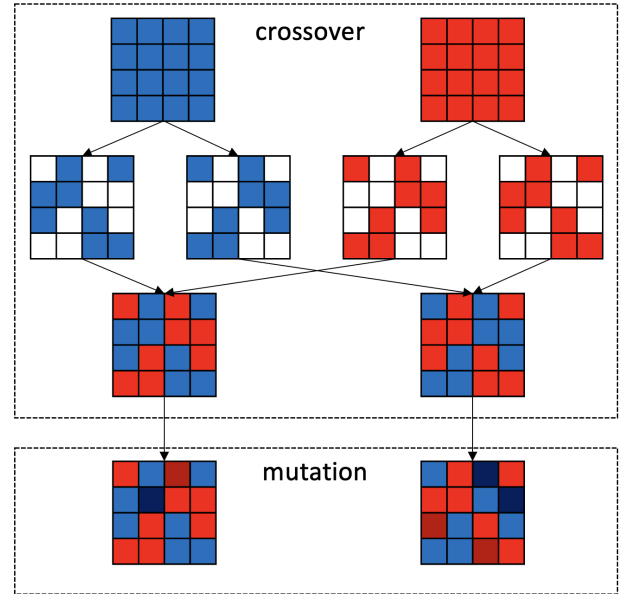


Figure 5: Illustration of crossover and mutation in GA

Crossover The crossover operator will combine a pair of parents from last step to generate a pair of children, which share many of the characteristics from the parents. The half elements of parents are randomly exchanged.

Mutation Some elements of children are randomly altered to add variance in the evolution. It should be noticed that the mutated samples should still fall into the norm ball $B(x, r)$. Finally, the children and parents will be the individuals for the next generation.

Termination The termination condition of GA is either maximum number of iterations is reached or the highest ranking of fitness reaches a plateau such that successive iterations no longer produce better results. In this paper, we fix the maximum iteration number for simplicity.

GA can be directly applied to the unconstrained optimisation when objective function equals to fitness function. The constraint optimisation is more challenging and different strategies are proposed to handle the non-linear constraint for GA (Michalewicz and Schoenauer 1996). One of the popular approaches is based on the superiority of feasible individuals to make distinction between feasible and infeasible solutions (Powell and Skolnick 1993).

9.3 Subset Simulation

Subset Simulation (SS) is widely used in reliability engineering to compute the small failure probability. The main idea of SS is introducing intermediate failure events so that the failure probability can be expressed as the product of larger conditional failure probabilities (Au and Beck 2001).

Suppose the distribution of perturbed inputs with the norm ball is $q(x)$, and the failure event is denoted as F . let $F = F_m \subset F_{m-1} \subset \dots \subset F_2 \subset F_1$ be a sequence of increasing events so that $F_k = \bigcap_{i=1}^k F_i$. By the definition of conditional probability, we get

$$\begin{aligned}
P_F &= P(F_m) = P\left(\bigcap_{i=1}^m F_i\right) \\
&= P(F_m | \bigcap_{i=1}^{m-1} F_i) P\left(\bigcap_{i=1}^{m-1} F_i\right) \\
&= P(F_m | F_{m-1}) P\left(\bigcap_{i=1}^{m-1} F_i\right) \\
&= P(F_m | F_{m-1}) \dots P(F_2 | F_1) P(F_1) \\
&= P(F_1) \prod_{i=1}^{m-1} P(F_{i+1} | F_i)
\end{aligned} \tag{19}$$

F_m is usually a rare event, which means a large amount of samples are required for the precise estimation by Simple Monte Carlo (SMC). SS decomposes the rare event with a series of intermediate events, which are more frequent. The conditional probabilities of intermediate events involved in Eq. (12) can be chosen sufficiently large so that they can be efficiently estimated. For example, $P(F_1) = P(F_{i+1} | F_i) = 0.1$, $i = 1, 2, 3, 4$, then $P_F \approx 10^{-5}$ is too small for the efficient estimation by SMC.

The keypoint of SS is estimating $P(F_1)$ and conditional probabilities $P(F_{i+1} | F_i)$. On the one hand, F_1 can be chosen as the common event such that by SMC of N perturbed inputs within the norm ball $x'_k \sim q(x')$, all samples fall into

F_1 . On the other hand, computing the conditional probability

$$P(F_{i+1} | F_i) = \frac{1}{N} \sum_{k=1}^N \mathbb{1}_{F_{i+1}}(x'_k) \approx \rho \tag{20}$$

requires the simulation of $(1 - \rho)N$ additional samples. For example, if we have N samples belonging to F_{i-1} with $i \geq 2$, and $P(F_i | F_{i-1}) = \rho$, which indicate ρN samples belongs to F_i . To estimate next conditional probability $P(F_{i+1} | F_i)$, $(1 - \rho)N$ additional samples lying in F_i should be simulated to expand the population size to N . Given the conditional distribution $q(x' | F_i) = q(x') I_{F_1}(x') / P(F_i)$, on average $1/P(F_i)$ samples are simulated before one such sample occur. The Markov Chain Monte Carlo based on Metropolis-Hastings (MH) algorithm can be adopted to improve the efficiency.

At intermediate iteration i , we already obtain ρN samples lying in F_i , that is $x' \in F_i$. The target distribution is $q(\cdot | F_i)$. We can use MH algorithm to generate new samples x'' from the proposal distribution $g(x'' | x')$. $g(x'' | x')$ can be normal distribution or uniform distribution centred at x' . The MH algorithm can be written as below:

Initialisation Pick up a sample x' belonging to F_i . Set step $t = 0$ and let $x_t = x'$.

Iteration At step t , generate a random candidate sample x'' according to $g(x'' | x_t)$. Calculate the acceptance probability

$$A(x'', x_t) = \min\left\{1, \frac{q(x_t | F_i) g(x_t | x'')}{q(x'' | F_i) g(x'' | x_t)}\right\} \tag{21}$$

and accept the new sample x'' with probability $A(x'', x_t)$. Further check if $x'' \in F_i$, otherwise reject x'' . In practice, we generate a uniform random number $u \in [0, 1]$, set x_{t+1} as

$$x_{t+1} = \begin{cases} x'' & \text{if } u \leq A(x'', x_t) \text{ and } x'' \in F_i \\ x_t & \text{Otherwise} \end{cases} \tag{22}$$

and increment $t = t + 1$.

We can run a large amount of Markov chains simultaneously to enlarge the set of i.i.d. samples falling into F_i . However, as discussed in (Katafygiotis and Zuev 2008; Schueller, Pradlwarter, and Koutsourelakis 2004), MH becomes inefficient for high dimensional problems. The acceptance probability $A(x'', x')$ will rapidly decrease with increasing dimensions. It results in many repeated samples and high correlated Markov chains. It is recommended to adapt the proposal distribution $g(x'' | x')$ after M steps of MH (Papaioannou et al. 2015). The mean acceptance probability should be kept around 0.234 (Gelman, Gilks, and Roberts 1997).

The whole process of SS can be summarized as follows. First, we simulate N perturbed samples within the norm ball $B(x, r)$ (all belong to F_1) and use SMC to estimate $P(F_2 | F_1)$. From these N samples, we already obtain ρN samples distributed from $q(\cdot | F_2)$. Start from each of these ρN samples falling in F_2 , we can create a Markov chain and run MH M steps to generate new samples distributed from $q(\cdot | F_2)$. In initial SS method (Au and Beck 2001), ρN distinct Markov chains (with different start points) are created.

$1/\rho$ new samples are drawn from each chain, and the covariance between new samples in same Markov chain should be considered for evaluating the coefficient of variation (c.o.v) of the final estimation on P_F . (C erou et al. 2012) modify the algorithm by firstly enlarge set to N samples with replacement from ρN . Then N Markov Chains are constructed and only one sample is drawn from each chain.

These new generated samples can be utilised to estimate $P(F_3|F_2)$. Repeating this process until the rare failure of interest. We get the final estimation of failure event probability by ‘‘assembling’’ the conditional probabilities with Eq. (12).

Statistical Property of SS Estimator We present the analysis on statistical property of \bar{P}_{F_i} (shortened notation for $\bar{P}(F_1)$ and $\bar{P}(F_{i+1}|F_i)$) and \bar{P}_F . They are based on the assumption that Markov chain generated by MH algorithm is theoretically ergodic. That is, the stationary distribution is unique and independent of the initial state. Since we use SMC with samples simulated from Markov chain to estimate \bar{P}_{F_i} (ref. to Eq. (20)), The coefficient of variation of \bar{P}_{F_i}

(c.o.v) is approximated by $\sqrt{\frac{1-\bar{P}_{F_i}}{\bar{P}_{F_i}N}}$. Finally, we can calculate estimated mean \bar{P}_F and c.o.v $\bar{\delta}$ as

$$\begin{aligned} \bar{P}_F &= \prod_{i=1}^m \bar{P}_{F_i} = \prod_{i=2}^m \frac{1}{N} \sum_{k=1}^N \mathbb{1}_{F_i}(x'_k) \\ \bar{\delta}^2 &\approx \sum_{i=2}^m \frac{1-\bar{P}_{F_i}}{\bar{P}_{F_i}N} \end{aligned} \quad (23)$$

where $\bar{P}_{F_1} = 1$. It should be noted that \bar{P}_F is biased for N , but asymptotically unbiased due to the fact that samples in F_i for computing \bar{P}_{F_i} are utilised to start Markov chain for computing $\bar{P}_{F_{i+1}}$.

9.4 Complexity Analysis of Genetic Algorithm and Subset Simulation Applied on XAI Methods

Although the proposed evaluation methods can be applied to all kinds of feature attribution based XAI techniques, the time complexity will be extremely high for perturbation based XAI methods, such as LIME and SHAP, which take random perturbation of input features to yield explanations.

The complexity of GA is $O(t \cdot N \cdot (c(\text{fitness}) + c(\text{crossover}) + c(\text{mutation})))$, where t and N are evolution iterations and population size, respectively. When we choose different XAI methods, the evaluation time of fitness values $c(\text{fitness})$ will change correspondingly.

The complexity of SS is related to the number of sub-events m , the number of MH steps M and number of simulated samples N . For estimating conditional probability of each sub-event, M MH steps are taken, and running each MH step requires the calculation of property function of N samples. Thus, the complexity of SS is approximately $O(m \cdot M \cdot N \cdot c(\text{property}))$. When we choose different XAI methods, the evaluation time of property function $c(\text{property})$ will change correspondingly.

From the definition of fitness function in GA and property function in SS, both $c(\text{fitness})$ and $c(\text{property})$ can be approximated by the computation of interpretation discrepancy

Table 3: Time counts of $N \cdot c(\text{cal_attr_dis})$ in seconds across different dataset ($N = 1000$). Results are averaged over 10 runs.

Dataset	Gradient x Input	Integrated Gradients	GradCAM	DeepLift	LIME	SHAP
MNIST	0.0202	0.0512	0.0342	0.0382	99.21	25.80
CIFAR-10	0.0909	0.3329	0.1222	0.1307	293.72	255.95
CelebA	0.0620	0.2759	0.0887	0.1029	739.59	692.75

$c(\text{cal_attr_dis})$. In practice, we can compute interpretation discrepancy in a batch, e.g. N samples can run simultaneously to generate the explanations. Therefore, we count the running time of $N \cdot c(\text{cal_attr_dis})$ across different datasets and different XAI methods in Nvidia A100. Results are presented in Table 3. LIME and SHAP take much more time than gradient-based XAI methods for the batch computation of interpretation discrepancy. This will be amplified by iteration number t in GA or number of sub-events times number of MH steps $m \cdot M$ in SS for one time evaluation of interpretation robustness.

9.5 Details of DL models

The information of DL models under evaluation are presented in Table 4. All experiments were run on a machine of Ubuntu 18.04.5 LTS x86_64 with Nvidia A100 GPU and 40G RAM. The source code, DL models, datasets and all experiment results are available at https://github.com/havelhuang/Eval_XAI_Robustness.

9.6 Experiment on Interpretation Discrepancy Measures

We study the quality of three widely used metrics, i.e. Mean Square Error (MSE), Pearson Correlation Coefficient (PCC), and Structural Similarity Index Measure (SSIM) (Dombrowski et al. 2019) to quantify the visual discrepancy between two attribution maps. The proposed evaluation methods can produce the adversarial interpretation with the guidance of different metrics. As shown in Fig. 6, the first row displays three seed inputs and corresponding attribution maps. The following groups separated by lines show the adversarial interpretation of perturbed input measured by different metrics. The value of PCC appears to be relatively more accurate in terms of reflecting the visual difference between original interpretation of seeds input and adversarial interpretations. Smaller PCC represents larger visual difference between two attribution maps. In addition, the value range of PCC is 0~1, with 0~0.3 indicating weak association, 0.5~1.0 indicating strong association. Therefore, it provides a uniform measurement across different seeds input and different dataset. In contrast, MSE can also precisely measure the visual difference but vary greatly with respect to seed inputs and image size. SSIM exhibits the worst performance in measuring difference between attribution maps.

9.7 Experiment on Parameter Sensitivity

Additional experiments on hyper-parameter settings in GA and SS are presented in Fig. 7 and Fig. 8. The objective function interpretation discrepancy \mathcal{D} , measured by PCC, is op-

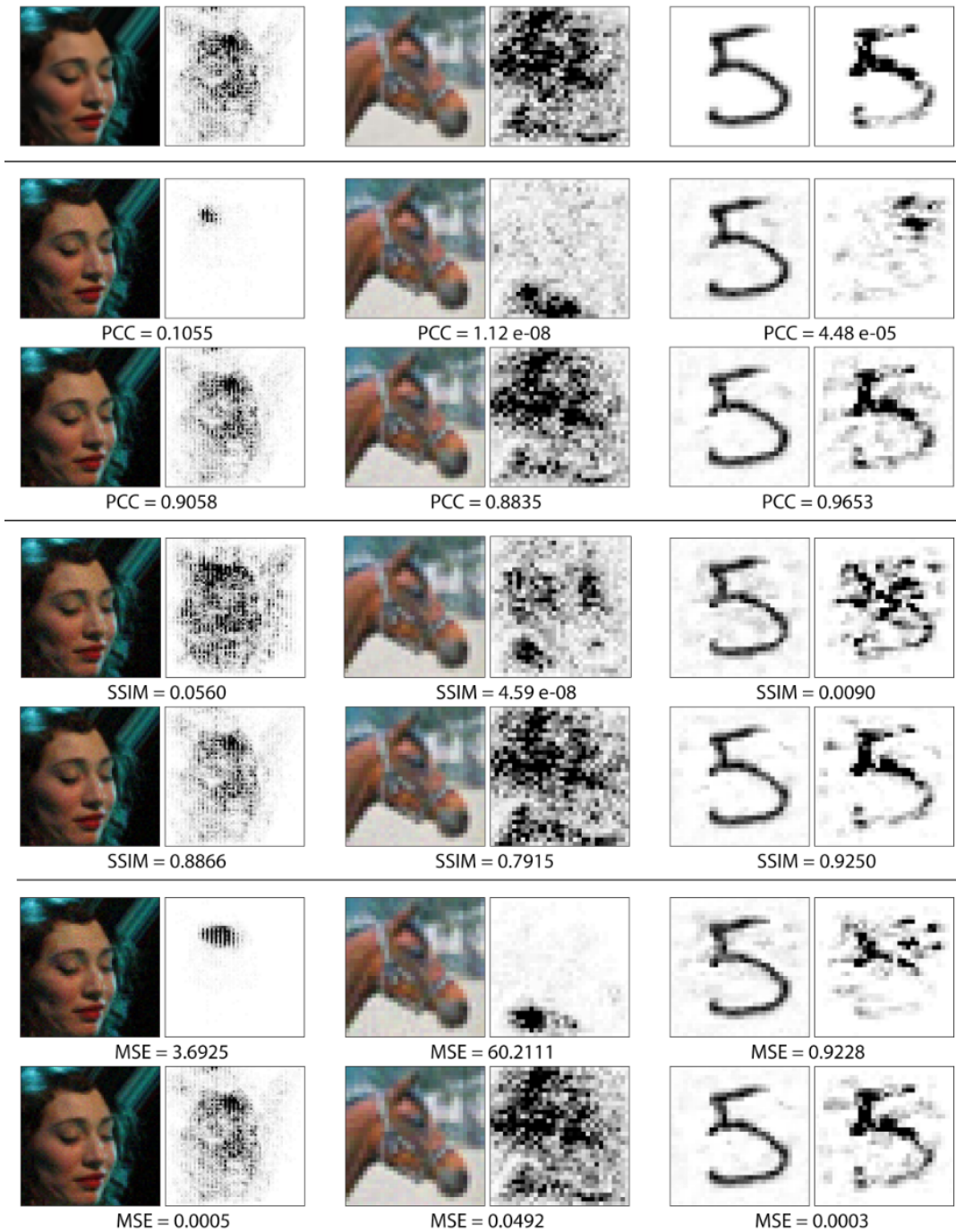


Figure 6: Comparison between PCC, SSIM and MSE as metrics of interpretation discrepancy between original interpretation and adversarial interpretation, generated by GA and SS. Smaller PCC, smaller SSIM, and larger MSE indicate greater difference. In this set of experiments, PCC is relatively the best to quantify the visual difference between attribution maps.

Table 4: Details of the datasets and DL models under evaluation.

Dataset	Image Size	r	DL Model	Org.		Grad. Reg.		Hess. Reg.		Adv. Train.	
				Train	Test	Train	Test	Train	Test	Train	Test
MNIST	$1 \times 32 \times 32$	0.1	LeNet5	1.000	0.991	0.993	0.989	0.993	0.989	0.994	0.989
CIFAR-10	$3 \times 32 \times 32$	0.03	ResNet20	0.927	0.878	0.910	0.876	0.786	0.779	0.715	0.703
CelebA	$3 \times 64 \times 64$	0.05	MobileNetV1	0.934	0.917	0.918	0.912	0.908	0.904	0.769	0.789

timised to converge with the increasing number of iterations while the prediction loss J as the constraint is gradually satisfied. The number of iterations in GA is more important than population size.

For hyper-parameters in SS, apart from the sensitivity of MH steps, we also discuss the impact of population size n and quantile ρ for conditional probability. As expected, increasing population size will improve the estimation precision, using SMC results with 10^8 samples as the ground truth. However, there is no exact answer for which ρ is better. In most cases, we find that $\rho = 0.5$ can reduce the estimation error, but will take more time for one estimation. Larger ρ represents more sub events are decomposed and additional estimation of conditional probability will obviously cost more time. Fortunately, we find SS estimation accuracy is more sensitive to the number of MH steps M and population size n , compared with ρ . Therefore, setting $\rho = 0.1$ but increasing MH steps and population size will get sufficiently accurate results. Finally, the rarity of failure events can determine the setting of these hyper-parameters. The estimating accuracy of more rare events, e.g. $PCC < 0.2$, is more sensitive to the theses parameters.

9.8 Experiments on Evaluating XAI methods

We evaluate the robustness of more XAI methods on CIFAR10 and CelebA dataset, including ‘‘Deconvolution’’, ‘‘Guided Backpropagation’’, ‘‘Gradient \times Input’’, ‘‘Integrated Gradients’’, ‘‘GradCAM’’, and ‘‘DeepLift’’. Results are presented in Fig. 9. In terms of misinterpretation with preserved classification, Integrated Gradients is the most robust XAI method due to the integral of gradient of model’s output with respect to the input. The integral averages the gradient-based attribution maps over several perturbed images instead of single point explanation. DeepLift has the similar smoothing mechanism by comparing the neuron activation with a reference point. Therefore, single point explanation like Deconvolution and GradCAM are vulnerable to this type of misinterpretation when DL model’s loss surface is highly curved, leading to the great change of gradients. Gradient \times Input is slightly better by leveraging the input sign and strength.

These XAI methods in general show similar robustness against misinterpretation conditioned on misclassification, although we find the single point explanation is a litter better than explanation averaged over several points under this circumstance. We guess the rarity of misclassification and misinterpretation make it difficult to find the perturbed input which have different attribution map with input seeds. Therefore, the averaged interpretation of perturbed input tend to be consistent with original interpretation.

In addition to evaluation on different datasets, we do ex-

Table 5: Robustness evaluation of XAI methods on different neural network architecture for CIFAR-10 dataset.

Model Architecture	Eval Metrics	Gradient x Input	Integrated Gradients	GradCAM	DeepLift
ResNet20	$sol_{\hat{F}}$	0.0166	0.0375	0.0044	0.0212
	$sol_{\hat{F}}$	0.8562	0.8308	0.8079	0.8551
	$\ln P_{\hat{F}}$	-20.32	-45.05	-35.93	-21.22
	$\ln P_{\hat{F}}$	-80.73	-87.64	-68.27	-81.81
MobileNetV2	$sol_{\hat{F}}$	0.0552	0.1167	0.0523	0.0712
	$sol_{\hat{F}}$	0.7689	0.7885	0.7085	0.7707
	$\ln P_{\hat{F}}$	-12.75	-34.99	-16.01	-8.70
	$\ln P_{\hat{F}}$	-70.32	-62.19	-82.17	-68.38
VGG16	$sol_{\hat{F}}$	0.0767	0.1227	0.1133	0.0206
	$sol_{\hat{F}}$	0.7813	0.8240	0.8637	0.8358
	$\ln P_{\hat{F}}$	-14.42	-53.48	-47.52	-44.25
	$\ln P_{\hat{F}}$	-59.74	-54.155	-49.90	-66.02
DLA	$sol_{\hat{F}}$	0.0737	0.0953	0.0078	0.0930
	$sol_{\hat{F}}$	0.7919	0.8111	0.2113	0.7983
	$\ln P_{\hat{F}}$	-8.48	-28.69	-4.31	-9.77
	$\ln P_{\hat{F}}$	-39.57	-37.74	-77.57	-36.40

periments on different neural network architectures for CIFAR10 dataset. Results in Table 5 shows that Integrated Gradients maintain the most robust XAI method to misinterpretation with preserved classification, invariant to the change of neural network architecture. However, the robustness to misinterpretation conditioned on misclassification varies according to the internal structure of neural network. GradCAM seems to be robust in most cases.

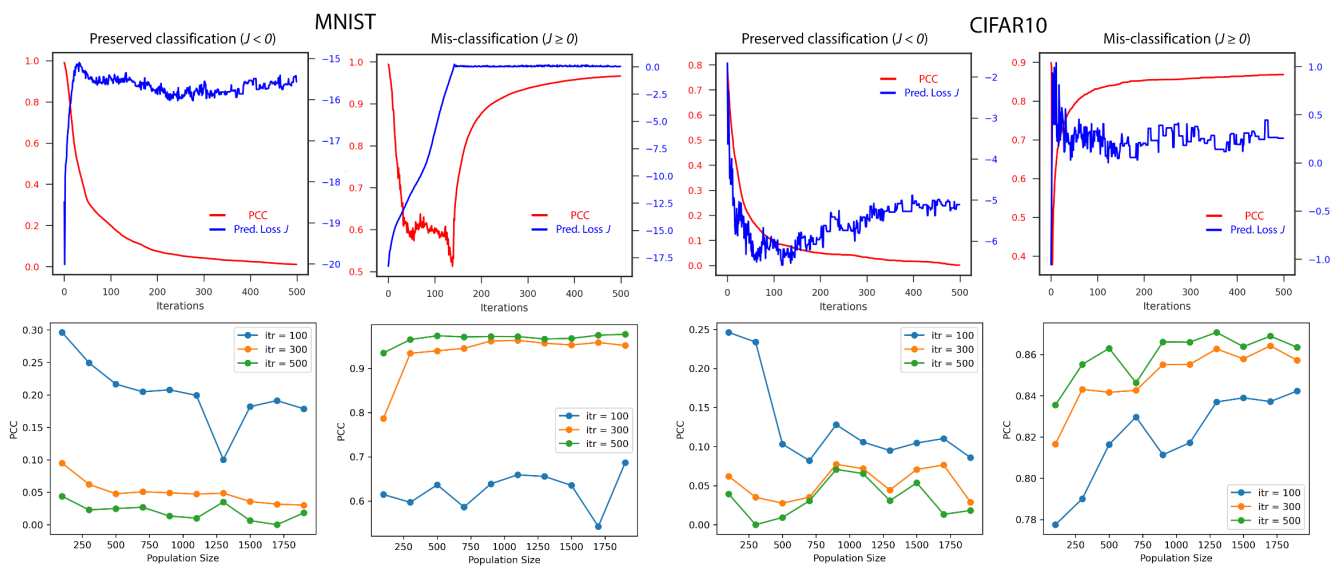


Figure 7: GA is applied to test seeds (norm balls) from MNIST and CIFAR10 dataset to find worst case interpretation discrepancy, measure by PCC. First row: fixed population size 1000, and varied iterations; Second row: fixed iterations, and varied population size. “Gradient×Input” interpretation method is considered.

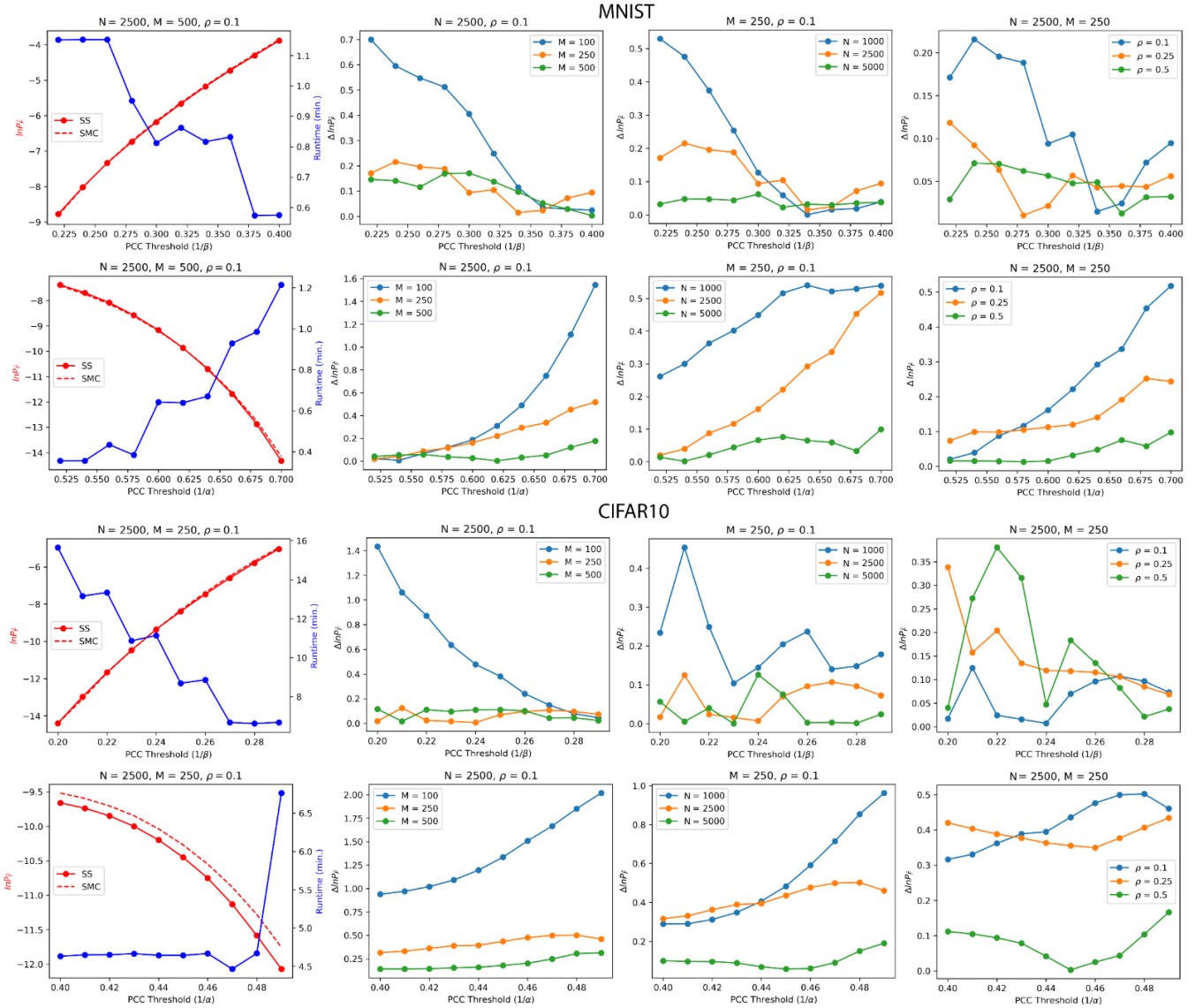


Figure 8: SS for estimating the probability of misinterpretation ($\ln P_F$) within a norm ball from MNIST, CIFAR10 dataset compared with SMC using 10^8 samples (22 minutes for each estimate for MNIST; 154 minutes for each estimate for CIFAR10). Results are averaged on 10 runs. “Gradient×Input” interpretation method is considered.

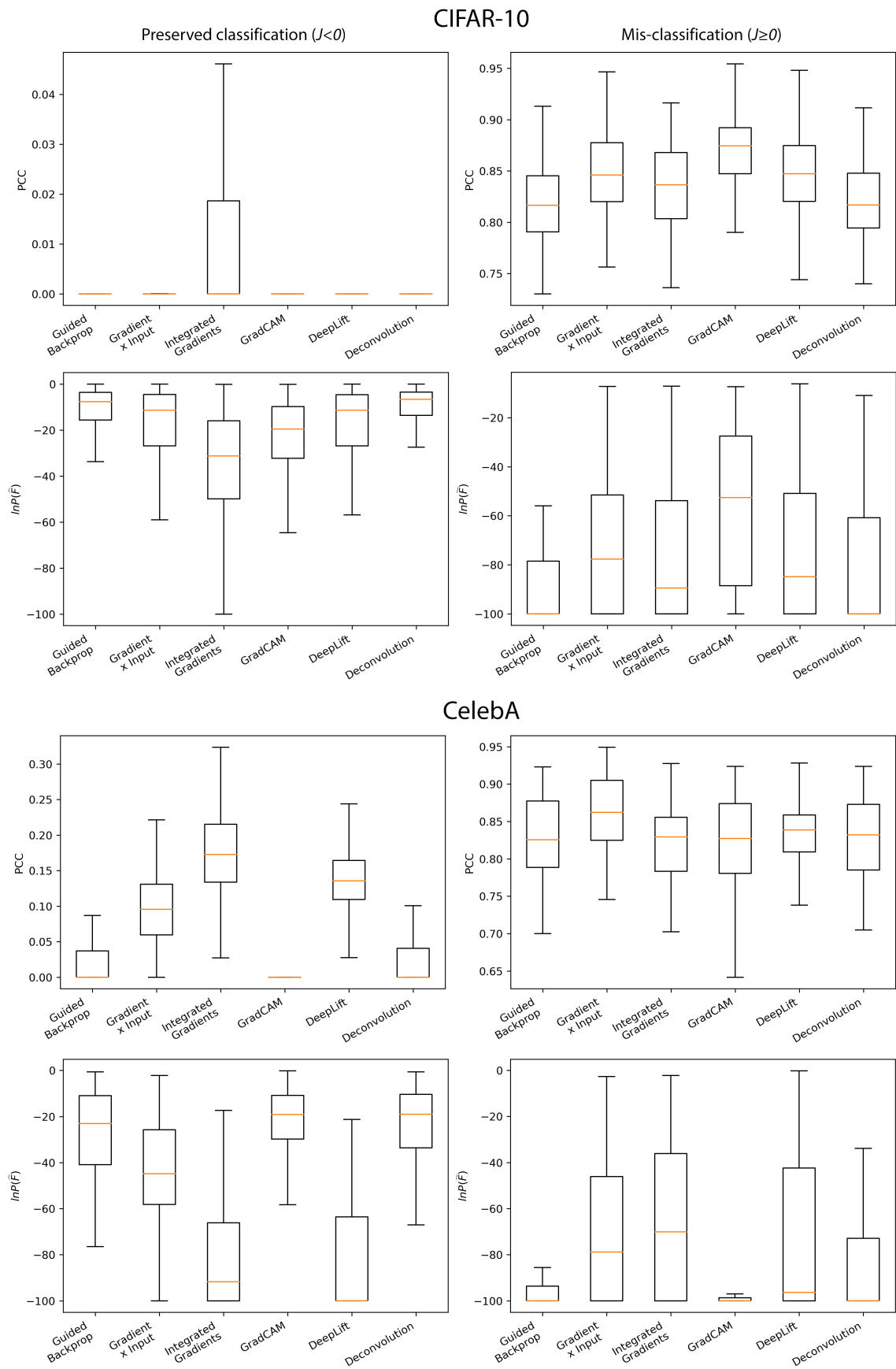


Figure 9: Robustness evaluation of different interpretation methods based on 100 randomly selected samples from CIFAR10 and CelebA test set. From top to bottom, first row (worst case evaluation) and second row (probabilistic evaluation). From left to right, first column (misinterpretation \hat{F}) and second column (misinterpretation \tilde{F})